Microstructure and Creep Strength of Welds in Advanced Ferritic Power Plant Steels

Fujio ABE and Masaaki TABUCHI
National Institute for Materials Science (NIMS)
1-2-1 Sengen, Tsukuba 305-0047, Japan

ABSTRACT

The microstructure and creep strength of simulated HAZ specimens and welded joints have been investigated for advanced 9-12%Cr steels in order to make clear the mechanisms responsible for Type IV crack and to improve creep strength of welded joints at high temperature. The creep and creep rupture tests were carried out at $650^{o}C$ (923 K) for up to about 10^4 h. The creep crack growth tests were also carried out for welded joints, base metal and simulated HAZ specimens using the CT specimens. The creep rupture time of simulated HAZ specimens has its minimum after heating to A_{C3} temperature, which produces fine-grained martensitic microstructure. Decreasing the width of HAZ by means of EB welding is effective for the extension of creep life but the brittle Type IV fracture appears even in the EB welded joints at low stress and long time conditions. Most of the welded joint specimens were fractured in fine-grained HAZ and resulted in shorter creep life than those of base metal due to the formation of creep voids and cracks. It should be also noted that in the fine-grained zone the recovery of martensitic microstructure during creep is inhomogeneous as shown by the formation of coarse subgrains in the region of fine subgrains. Using a specially-designed FEM code for Type IV crack growth behaviour, the vacancy diffusion under multi-axial stress condition in HAZ of welded joints is analyzed. The effect of creep ductility and void formation ahead of the crack tip on creep crack growth rate is successfully simulated.

1 INTRODUCTION

Since 1997, National Institute for Materials Science has been conducting the research and development of advanced ferritic steels for application to thick section boiler components such as main steam pipe and header of ultra-supercritical (USC) power plant at 650 ^{o}C (923 K).[1] Critical issues for the development of ferritic steels for 650 ^{o}C USC boilers are the improvement of oxidation resistance as well as long-term creep rupture strength. The resistance to Type IV cracking strength loss in welded joints is also serious for construction of thick section boiler components. Furthermore, the thermal cycling capabilities of thick section components in USC plant would be severely restricted by fatigue damage. Under these circumstances, our project involves the improvement of creep strength, oxidation resistance and creep-fatigue properties for high-Cr ferritic steels, including welded joints.

The softening zone and the fine-grained zone are produced in the heat affected zone (HAZ) of welded joints during heat cycle of welding, which accelerates microstructure evolution and damage development during creep. This is called Type IV creep fracture and reduces the creep life of welded joints of high-Cr ferritic steels at high temperature and low stress conditions.[2, 3] It is reported for 9Cr-1MoVNb steel that the creep rupture strength of welded joints is lower than that of base metal and that the difference in creep rupture strength becomes more significant with increasing temperature, especially above 600°C (873 K).[4] At present, however, the mechanisms responsible for a drop of creep rupture strength in the welded joints are not fully understood.

The purpose of the present research is to investigate the microstructure evolution, creep deformation and creep fracture behaviour in the HAZ and to clarify the mechanisms responsible for a drop of creep rupture strength in the welded joints for tungsten-strengthened advanced 9-12%Cr steels, ASME-P92 (9Cr-0.5Mo-1.8W-VNb), ASME-P122 (11Cr-0.4Mo-2W-CuVNb) and newly developed 9Cr steels in our Ultra-Steel project [1]. The creep and creep crack growth tests were carried out at 650°C (923 K) for up to about 10^4 h for simulated HAZ specimens and welded joints. Although the HAZ of real welded joints is limited to only a small volume, uniform microstructure can be obtained throughout creep specimens for the simulated HAZ materials.

2 EXPERIMENTAL PROCEDURE

The materials examined were ASME-P92 (9Cr-0.5Mo-1.8W-VNb) and ASME-P122 (11Cr-0.4Mo-2W-CuVNb) and newly developed 9Cr steels in our Ultra-Steel project. [1] The chemical compositions of ASME-P92 and ASME-P122 are given in Table 1. Plates of about 30 mm thickness were subjected to normalizing {at 1070°C (1343K) for 2 h (7.2ks) and at 1050°C (1323 K) for 100 min for P92 and P122, respectively} and tempering {at 780°C (1053K) for 2 h (7.2ks) and at 770°C (1043 K) for 6 h for P92 and P122, respectively}. Figure 1 shows the heat treatment conditions for the preparation of simulated HAZ samples. At a heating rate of 0.33 K/s, corresponding to 20 K/min, the A_{C1} temperature was found to be about 850°C (1123K) and 820°C (1093 K) for P92 and P122, respectively, while the A_{C3} temperature was about 920°C (1193 K) for both the steels. The simulated HAZ specimens were kept for 180 s at various peak temperatures between 850 (1123) and 1000°C (1273 K) and then cooled in air. Finally, the post weld heat treatment (PWHT) was carried out for each specimen including the base metal at 740°C (1013K) for 4.7 h (16.8 ks). The welded joints were prepared basically by means of Gas Tungsten Arc (GTA) welding. The procedure conditions of multi-layers GTA welding are given in Table 2. The welded joints were also subjected to the PWHT similar to the simulated HAZ specimens.

Creep and creep rupture tests were carried out at 650°C for up to 10^4 h, using specimens of 6 mm gauge diameter and 30 mm gauge length for the simulated HAZ specimens and of 17.5 x 5mm cross section and 100 mm gauge length for the welded joints as shown in Figure 2(a). The longitudinal direction of the creep specimens was parallel to the rolling direction of the plate for the simulated HAZ specimens and perpendicular to the welding direction for the welded joints. The microstructure of the longitudinal cross section of the creep specimens was observed by scanning and transmission electron microscopes. The Vickers hardness was measured on the longitudinal cross section of the specimens at a load of 4.9 N at room temperature.

Table 1　Chemical compositions of ASME-P92 and ASME-P122 examined.

(mass %)

	C	Si	Mn	P	S	Cu	Cr	Mo	W	V	Nb	B	N
P92	0.09	0.16	0.47	-	-	-	8.72	0.45	1.87	0.21	0.06	0.002	0.050
P122	0.12	0.28	0.61	0.018	0.001	0.97	10.5	0.36	2.05	0.21	0.06	0.003	0.069
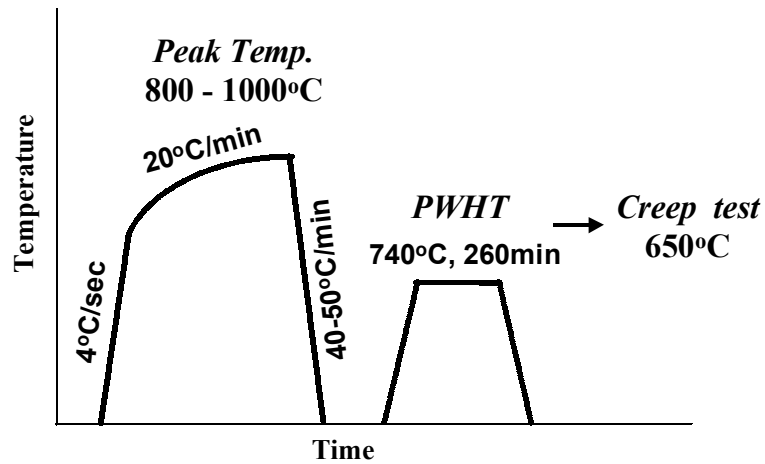
Figure 1   Heat treatment conditions for simulated HAZ specimens.

(a) creep test specimen

Table 2   Procedures of welded joints.

groove	single bevel 20 deg
pre-heating	> 373 K
welding current	200-250A
arc voltage	10-10.5V
welding speed	1.2-1.5mm/s
multi-layer	33-37pass
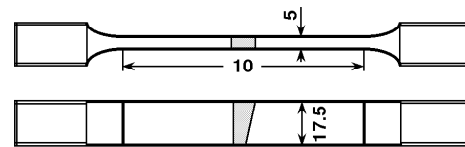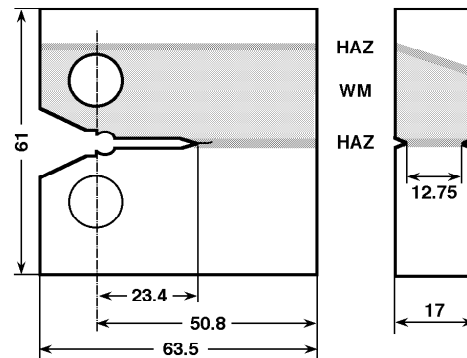
(b) CT specimen

Figure 2   Specimens of welded joints.

The creep crack growth tests were also carried out for welded joints, base metal and simulated HAZ specimens using the CT specimen shown in Figure 2(b).   The notch tip of welded joint CT specimen was located in HAZ.   The fatigue pre-crack of 3mm and 25% side-groove in thickness was induced.   Crack length was measured by D.C. electrical potential method.

3   RESULTS AND DISCUSSION

3.1 CREEP STRENGTH AND MICROSTRUCTURE OF SIMULATED HAZ SPECIMENS

In order to clarify the mechanisms of Type IV crack in welded joints, the relationship between creep strength and microstructure has been investigated for P92 and P122 after heat treatments simulating HAZ of welded joints.[5-8]   Figure 3 shows the time to rupture of P122 at 650 $^\circ$C and Vickers hardness at room temperature before creep tests, as a function of peak temperature in simulated heating.   The creep rupture time has its minimum after heating the specimens to the temperature near A_{C3}, while the hardness has its minimum after heating to the temperature near A_{C1}.   Therefore, the softening pronounced by the A_{C1} heating does not explain the minimum time to rupture.   The prior austenite grain size decreased with increasing peak temperature up to 950 $^\circ$C, indicating that the A_{C3} heating resulted in much more fine grains than the base material and A_{C1} heating.   The present results indicate that the fine grains produced by the A_{C3} heating are responsible for the minimum time to rupture.
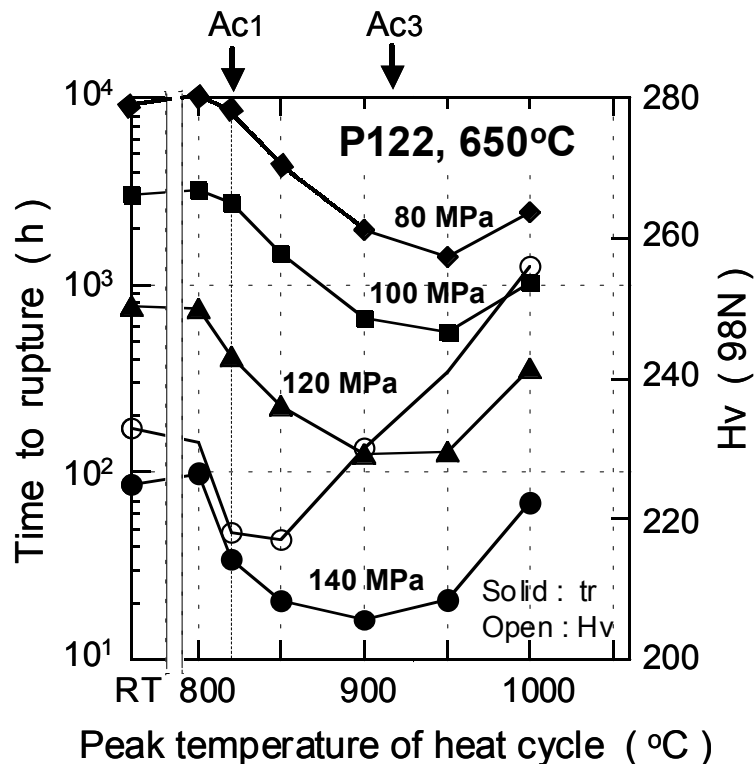

Figure 3   Time to rupture at 650°C and Vickers hardness at room temperature of simulated HAZ specimens of P122, as a function of peak temperature of heat cycle simulation.

Similar to P122, the simulated HAZ specimens of P92 exhibit that the creep rupture time has its minimum after heating the specimens to the temperature near A_{C3}.   But, the hardness also has its minimum after the A_{C3} heating, although there is not large difference in hardness between the A_{C1} and A_{C3} simulated HAZ specimens.   Hasegawa and co-workers [3] already reported the similar results on P92.

The creep deformation behaviour and microstructure evolution during creep have been examined for the A_{C1} and A_{C3} simulated HAZ specimens of P122 at 650°C, comparing with those of base metal.   This is shown in Figure 4.   At a high stress of 140 MPa, the time to rupture of the A_{C1} simulated HAZ specimen is rather similar to that of the A_{C3} simulated HAZ specimen but much shorter than that of base metal.   With decreasing stress and increasing
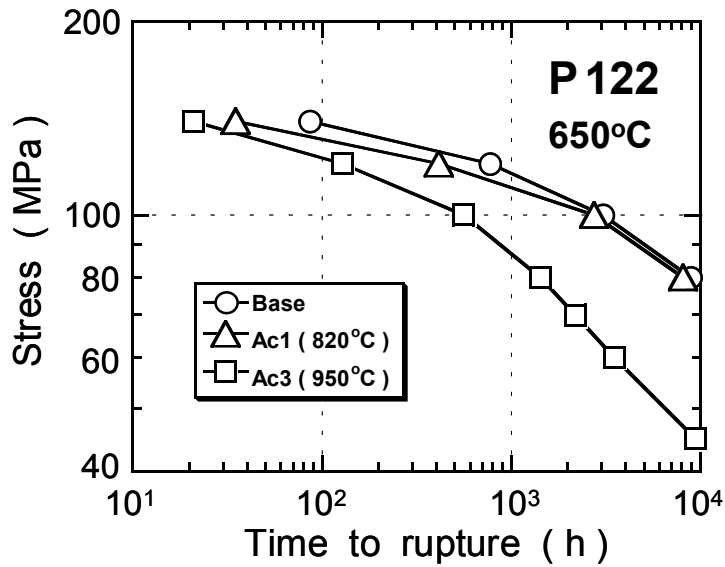
Figure 4   Creep rupture data for the Ac_1 and Ac_3 simulated HAZ specimens and base metal of P122 at 650°C.

test duration, the difference in time to rupture between the Ac_1 simulated HAZ specimens and base metal becomes decreased and substantially disappears at low stresses below 100 MPa, while that between the Ac_3 simulated HAZ specimens and base metal becomes increased. The decrease in creep rupture strength with decreasing stress, corresponding to the slope of the curves, becomes more significant with increasing time.   The stress dependence of time to rupture correlates with the stress dependence of minimum creep rate.   This is shown in Figure 5, where the minimum creep rate of the Ac_1 and Ac_3 simulated HAZ specimens and base metal is shown as a function of stress at 650°C.   At low stresses below 100 MPa, the
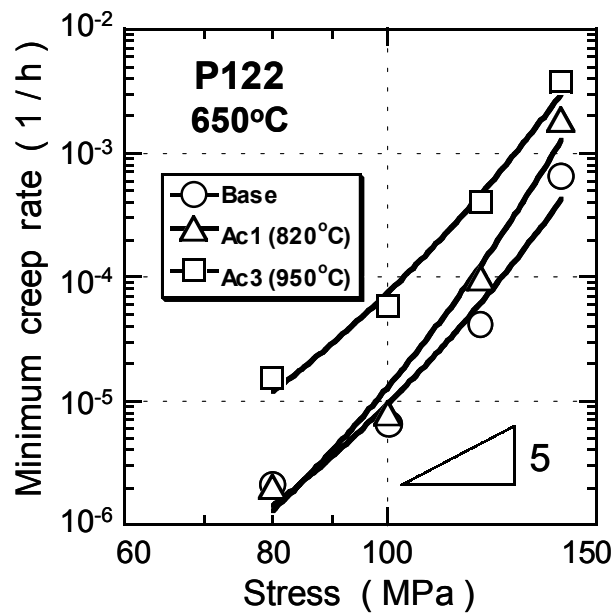

Figure 5   Stress dependence of minimum creep rate of the Ac_1 and Ac_3 simulated HAZ specimens and base metal of P122 at 650°C.

minimum creep rate is substantially the same between the Ac_1 simulated HAZ specimens and base metal, while that that of the Ac_3 simulated HAZ specimens is much higher than that of the Ac_1 simulated HAZ specimens and base metal.   It should be also noted that the stress exponent n of Norton's law given by $\dot{\varepsilon}_{min} = A\,\sigma^{\,n}$, where A and n are constants, is evaluated to be larger than 5.   With pure, close-packed metals, the value of n is known to be between 4 and 6 over a wide range of applied stress.[9]   Very large n values up to 40 have been reported by Williams and Wilshire [10] for complex alloys consisting of two or more phases.

Figure 6 shows the creep rate versus time curves of the Ac_1 and Ac_3 simulated HAZ specimens and base metal at 650°C and 100 MPa.   The creep rate curves consist of the primary or transient creep region, where the creep rate decreases with time, and of the tertiary or acceleration creep region, where the creep rate increases with time after reaching a minimum creep rate.   There is substantially no steady-state region, where the creep rate is constant.   In the initial stage of creep, the creep rate is substantially the same among the 3 specimens subjected to different treatments.   It should be noted that the transient creep region of the Ac_1 simulated HAZ specimen and base metal continues up to longer times than that of the Ac_3 simulated HAZ specimen.   In other words, the onset of acceleration creep of the Ac_1 simulated HAZ specimen and base metal is retarded up to longer times than that of the Ac_3 simulated HAZ specimen.   The longer duration of transient creep and hence the retardation of acceleration creep results in the lower minimum creep rate and longer rupture time.
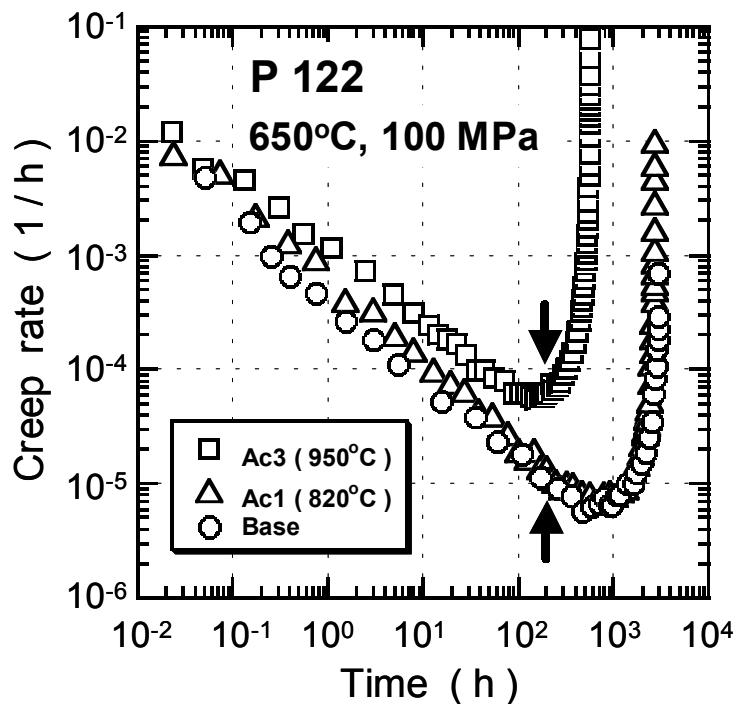

Figure 6   Creep rate versus time curves of the Ac_1 and Ac_3 simulated HAZ specimens and base metal of P122 at 650°C and 100 MPa.

In order to make clear the reason why the onset of acceleration creep is promoted in the Ac_3 simulated HAZ specimen, the microstructure evolution during creep was observed after interrupting creep test at a time at which the creep rate exhibits a minimum value as shown by
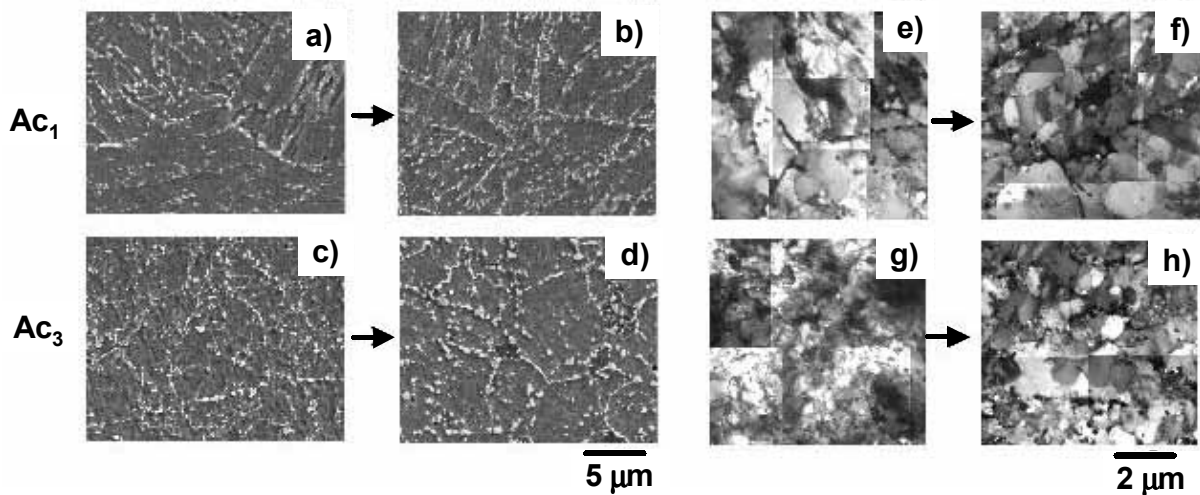
Figure 7　Microstructure of the Ac_1 and Ac_3 simulated HAZ specimens of P122 after creep deformation for 200 h at 650°C and 100 MPa.

the arrow in Figure 6.　This is shown in Figure 7, where the SEM and TEM micrographs of the Ac_3 simulated HAZ specimen before and after creep for 200 h at 650°C and 100 MPa are compared with those of the Ac_1 simulated HAZ specimen.　At the condition of creep for 200 h, the Ac_1 simulated HAZ specimen has not reached a minimum creep rate as can be seen from Figure 6.　After heat treatment simulating HAZ and before creep test, the Ac_3 simulated HAZ specimen is observed to be fine-grained martensitic microstructure containing high density of dislocations and large $M_{23}C_6$ carbides but substantially no lath distribution. The martensitic microstructure without lath distribution is quite different from that of the base metal and Ac_1 simulated HAZ specimens.　The lath martensitic microstructure of the Ac_1 simulated HAZ specimen is similar to that of the base metal but dislocation density is rather lower than in the base metal.　The Ac_1 heating corresponds to tempering treatment at higher temperature, which causes a recovery of excess dislocations rather homogeneously during tempering.　During creep at 650°C, the coarsening of $M_{23}C_6$ carbides and the inhomogeneous recovery of excess dislocations are more significant in the Ac_3 simulated HAZ specimen than in the Ac_1 simulated HAZ specimen.　The higher dislocation density after the Ac_3 heating promotes the inhomogeneous recovery of microstructure during creep, producing weak or soft region inhomogeneously.　This promotes the onset of acceleration creep for the Ac_3 simulated HAZ specimen, resulting in higher minimum creep rate and shorter time to rupture than for the metal and Ac_1 simulated HAZ specimens.　The change in microstructure due to the Ac_1 and Ac_3 heating treatments observed in P122 was also typical for P92.

The microstructure evolution during PWHT after the Ac_3 heating treatment was examined for P92 by TEM observations of extraction replicas.　This is shown in Figure 8.　By heating up to Ac_3 in a short time, most of precipitates dissolve in the matrix, however, some of the precipitates are still remained.　These undissolved precipitates are coarsened during PWHT. The large size of $M_{23}C_6$ carbides above 500nm can be observed in Figure 8(b).　In addition to these coarsened $M_{23}C_6$ carbides, small size $M_{23}C_6$ carbides below 100nm are newly precipitated.　The size of MX seems to be not changed during PWHT.　The sparse distribution of coarsened $M_{23}C_6$ carbides has a correlation with the degradation of creep rupture time of the Ac_3 simulated HAZ specimens.

before PWHT   after PWHT
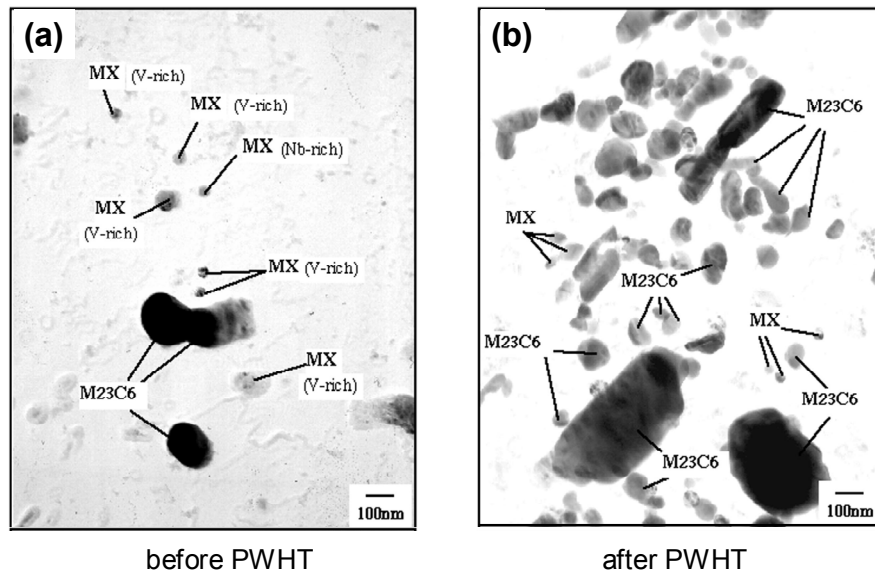
Figure 8   Extraction replicas of Ac_3 simulated HAZ specimens of P92.
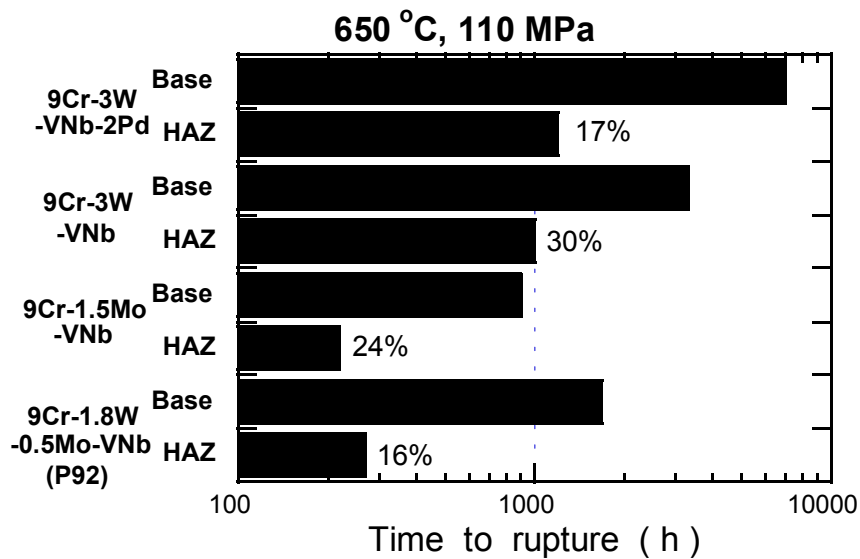

Figure 9   Creep rupture data of base metal and A_{C3} simulated HAZ specimens
for the steels at 650°C and 110 MPa.

Figure 9 compares the creep rupture time of A_{C3} simulated HAZ specimens among 9Cr-3WVNb steels with and without 2Pd, 9Cr-1.5MoVNb steel and P92 at 650°C and 110 MPa, where the results of base metal are also shown for comparison.[11]   The ratio of the creep rupture time of A_{C3} simulated HAZ to that of base metal is ranging from about 20 to 30%. Therefore, the creep rupture time of A_{C3} simulated HAZ is proportional to that of base metal, suggesting that the improvement of creep strength for base metal contributes to the improvement of creep strength for welded joint.

3.2 CREEP STRENGTH AND FRACTURE BEHAVIUOR OF WELDED JOINTS

Figure 10 shows the creep rupture data for the smooth plate specimens of welded joints and for round bar specimens of weld metal, base metal and A_{C3} simulated fine-grained HAZ at 650°C. [8] The creep rupture time is longer in the order of weld metal, base metal, EBW joint, GTAW joint with U-groove, GTAW with single bevel groove and A_{C3} simulated HAZ. The creep rupture data of the GTAW and EBW joints are located between those of the base metal and A_{C3}-simulated HAZ specimens. Welded joint specimens were all fractured in the fine-grained HAZ (Type IV fractured) except for one the EBW joint tested at 110 MPa that was fractured in the base metal. Further the rupture times of Type IV fractured joints were lower than that of base metal, which becomes more significant with decreasing stress. In order to improve the creep strength of welded joints, the width of HAZ was successfully reduced by means of EBW. The width of HAZ was 2.5 and 0.5mm for the conventional GTAW and EBW welded joints, respectively. The rupture times of the EBW joints are longer than those of the GTAW joints by about 2 times. The present results indicate that decreasing the width of HAZ is effective for the extension of creep life but that the brittle Type IV fracture appears even in the EBW joints at low stress and long time conditions. Figure 11 shows the profile of cracked EBW joint crept for 7300 h at 60 MPa. Creep cracks initiate near the surface of joints and propagate towards the center of thickness along the fine-grained HAZ region that would be heated to Ac_3 temperature during welding. In the SEM micrographs, the fine transgranular precipitates, which would contribute to creep strength, are distributed along lath boundaries in the base metal. In the A_{C3} simulated fine-grained HAZ, the coarse precipitates of $M_{23}C_6$ and $Fe_2(W, Mo)$ Laves phase are distributed along grain boundaries, while fine transgranular precipitates are not observed. The coarsening of intergranular precipitates during creep is more significant in the fine-grained HAZ than in other regions as shown in Figure 12, where the TEM micrographs of base metal and fine-grained zone in HAZ of P122 GTAW joint before and after creep for 3700 h at 650°C and 60 MPa are shown. The recovery of excess dislocations is also
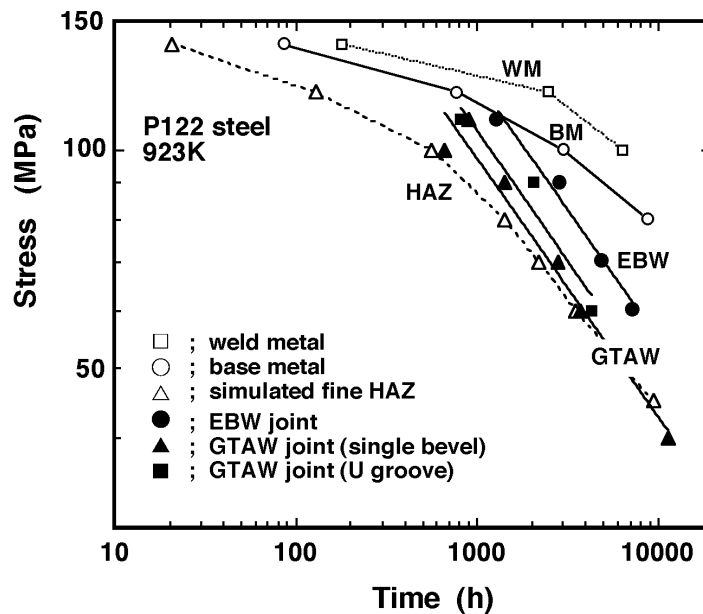

Figure 10   Creep rupture data for weld metal, base metal, A_{C3} simulated fine-grained HAZ, GTA and EB welded joints of ASME-P122 at 650°C.

significant in the fine-grained HAZ. These cause the degradation of creep strength of welded joints.

Creep voids are frequently observed at the interface between intergranular precipitates and matrix ahead of the crack tip.   The type IV creep crack grows accompanied by creep voids, as shown in Figure 11.   Creep deformation of fine-grained HAZ with lower creep strength is mechanically constrained by weld metal and base metal with higher creep strength. Vacancy diffusion, the formation and growth of voids will be accelerated under multi-axial condition for the welded joint specimens.[12]   The creep crack growth is also accelerated by void formation ahead of the crack tip.[13, 14]   In order to evaluate the vacancy diffusion under multi-axial stress condition, we have conducted computational analysis, which will be described in section 3.3.
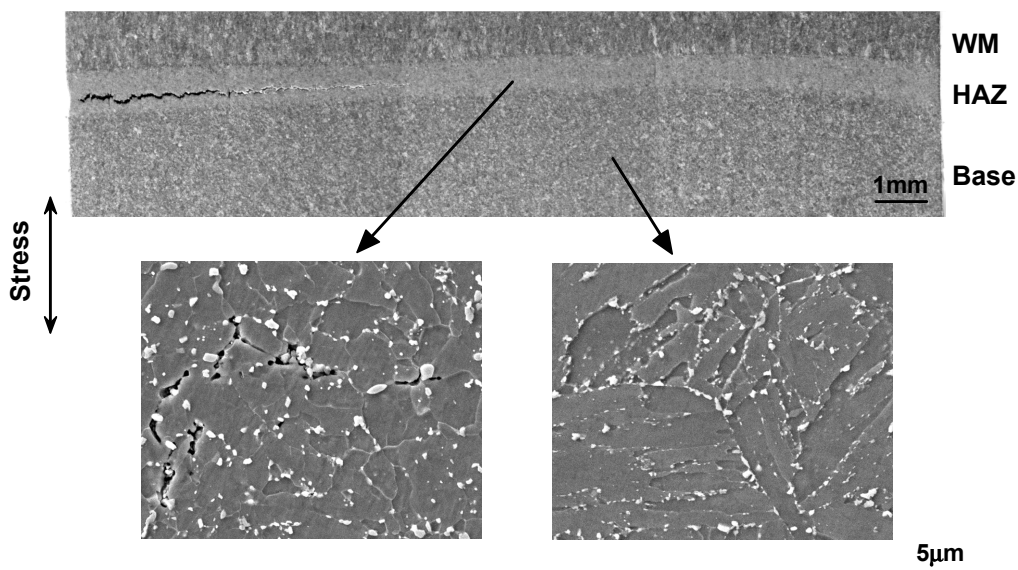

Figure 11   Profile and microstructures of creep cracked EBW joint
of P122 after creep rupture testing at 650°C and 60 MPa (tr = 7300 h).

It should be noted that the coarse subgrains of several μm, where the recovery of microstructure has already occurred, are produced during creep in the fine-grained HAZ of both P92 and P122.   The recovery of higher density of dislocations to prior austenite grain boundaries in the fine-grained zone promotes the production of coarse subgrains in the vicinity of prior austenite grain boundaries.   The sparse distribution of large $M_{23}C_6$ carbides in the fine-grained zone can also promote the recovery of microstructure.   The inhomogeneous recovery of microstructure producing the coarse subgrains in the vicinity of prior austenite grain boundaries accelerates the production of weak or soft region.   This results in the concentration of creep deformation in the fine-grained zone and hence the formation of a large number of creep voids along grain boundaries, accelerating eventual creep fracture.   The degradation mechanisms of creep strength in the fine-grained HAZ of welded joint are considered to be similar to the simulated HAZ specimens.

The analysis of long term creep data of Mod.9Cr-1Mo and 12Cr steels in the NIMS Creep Data Sheets suggests that special attention should be paid to stabilize the microstructure in the vicinity of prior austenite grain boundaries for the improvement of long term creep strength.[1]

| before creep | crept for 3700h | before creep | crept for 3700h |

base metal

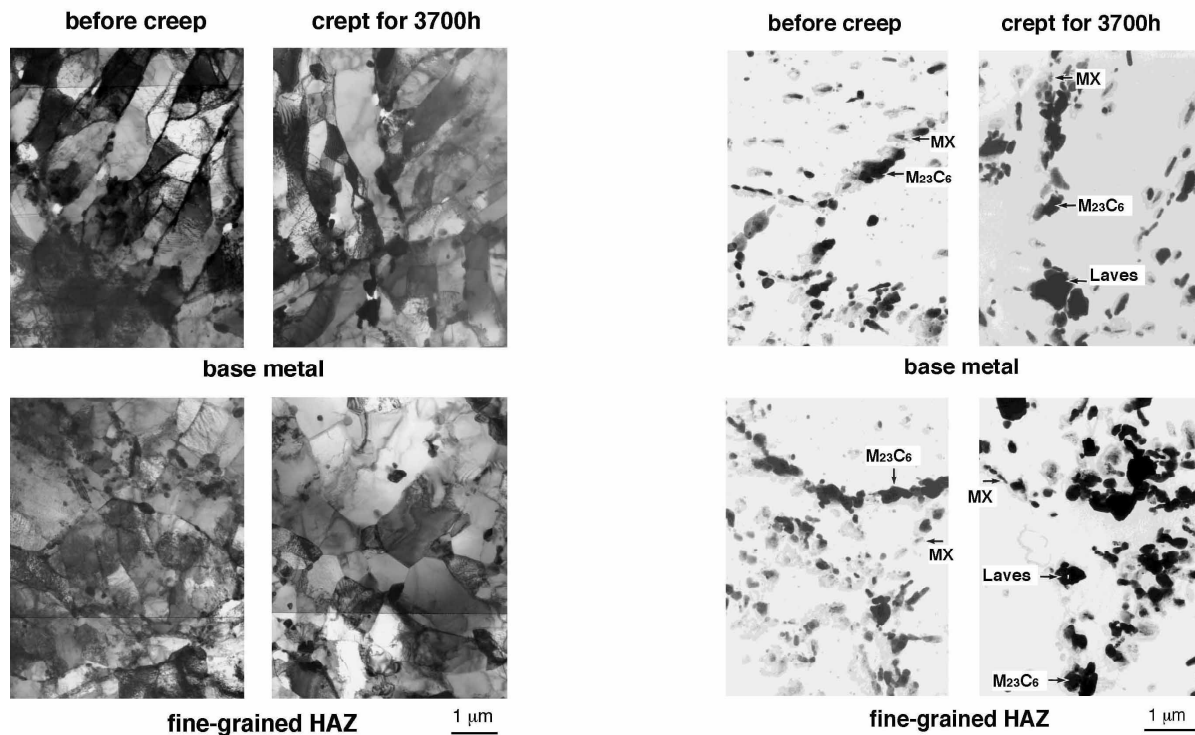fine-grained HAZ   1 μm

Figure 12   TEM micrographs of thin foils and replicas for base metal and fine-grained zone in HAZ of P122 GTAW joint before and after creep for 3700 h at 650°C and 60 MPa.

The TEM observations show that preferential recovery of martensitic microstructure has proceeded in the vicinity of prior-austenite grain boundaries in the specimens creep-ruptured at low stresses and long times above 10^4 h.   Because the fine-grained zone in HAZ contains a large number of grain boundaries, the stabilization of microstructure in the vicinity of grain boundaries should be strongly required for the improvement of long term creep strength for welded joints.   For example, we have confirmed that the addition of small amount of boron causes the stabilization of lath martensitic microstructure in the vicinity of prior austenite grain boundaries during creep through the stabilization of $M_{23}C_6$ carbides by an enrichment of boron.

3.3 COMPUTATIONAL SIMULATION OF TYPE IV CREEP CRACK GROWTH

Based on the observation shown in Figure 11, we have attempted to simulate Type IV creep crack growth behaviour taking the diffusive growth of creep voids into account. [5-6, 8] At first, creep crack growth is computed by the following method.   The creep crack growth could be characterized by critical strain criteria ahead of the crack tip. [14, 15]   The creep strain distribution of CT specimen model shown in Figure 13 is calculated by FEM using Norton's creep constitutive equation shown in Table 3.   When the equivalent creep strain ahead of the crack tip reaches to the critical value, which is the creep ductility of round bar specimen, the coordinate of the crack tip node is moved according to the method proposed by Hsu and Zhai. [16]   The C^* line integral in the path shown in Figure 13 is calculated for each time step.

A comparison of computational simulation and experimental results of creep crack growth rate da/dt versus C^* parameter for P122 base metal is shown in Figure 14.   The symbols
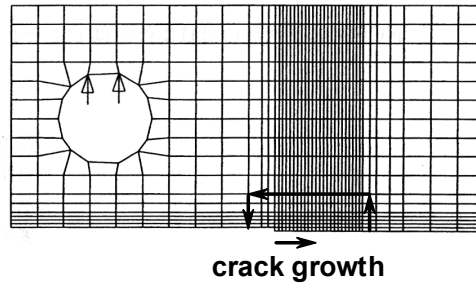
crack growth

Figure 13   2D analytical model for creep crack growth.

Table 3   Mechanical properties of P122 at 923K.

	E (GPa)	A (MPa^{-n} h^{-1})	N
Weld metal	106	2.45×10^{-36}	14.8
Coarse HAZ	99	4.86×10^{-22}	8.4
Fine HAZ	77	4.58×10^{-20}	7.7
Base metal	103	1.35×10^{-25}	10.0

indicate the relations between experimental da/dt versus experimental C^* obtained using displacement rate.   The dashed line shows the relations between computational da/dt versus C^* integral calculated by FEM.   The crack growth rate can be predicted from Norton's creep rule and creep fracture strain, because creep elongation of the present steel is about 20%.   If we use half value of fracture strain for fracture criteria, the twice value of da/dt is obtained as shown in Figure 14.   The computational simulation coincides with the experimental results that da/dt is inversely proportional to creep ductility.[15]
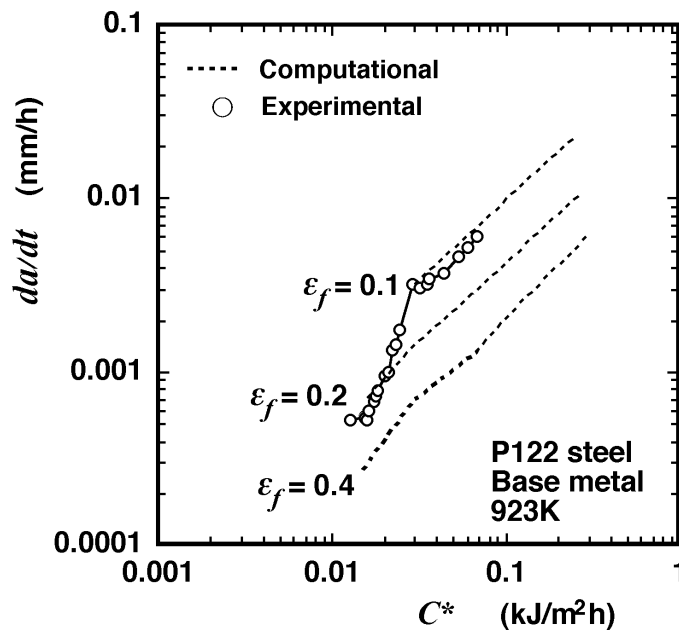

Figure 14   Comparison of experimental and computational da/dt for P122 base metal.

Three-dimensional FE model and equivalent creep strain contour is shown in Figure 15. In this case, creep crack grows faster in the center of specimen thickness than in specimen surface due to the three-dimensional constraint effect.   Figure 16 compares the experimental and computed creep crack growth curves of simulated HAZ, GTAW joint and base metal of P122.   Computed curves are obtained using the 3D model of Figure 15 and the creep parameters for fine-grained HAZ and base metal by assuming that the critical strain is 10%. Although the effect of mesh configuration exists for this analysis, the tendency of crack growth life is simulated.
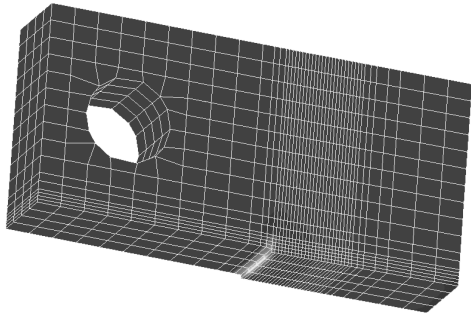

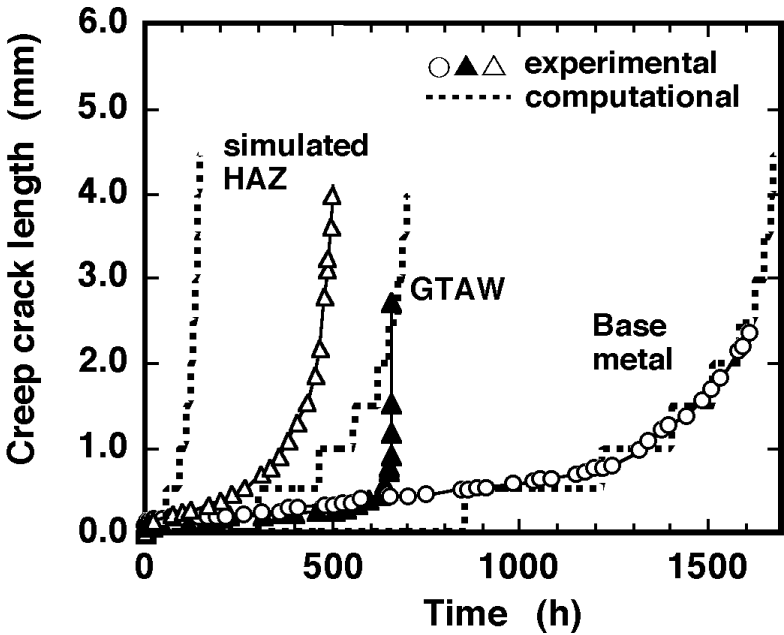Figure 15   3D model and equivalent creep strain contour.

Figure 16   Experimental and computational creep crack growth curve of P122 welded joint.

In order to evaluate the effect of vacancy diffusion under multi-axial stress condition, we conducted the following calculations.   The vacancy diffusion equation under multi-axial condition is given as follows [17] :

$$\frac{\partial C}{\partial t} = D\,\nabla\left(\nabla C + \frac{C}{RT}\nabla v\right) \tag{1}$$

$$v = -\,\sigma_p\,\Delta V \tag{2}$$

where, C is the vacancy concentration, D is the diffusion coefficient, R is the gas constant, T is the absolute temperature, σ_p is the hydrostatic stress and ΔV is the volume changes by vacancy diffusion. In this equation, the vacancy diffusion is controlled by hydrostatic stress gradient. In order to simulate realistic vacancy diffusion and concentration, weight coefficient α_1 and α_2 are added to Eq.(1) as follows [18] ;

$$\frac{\partial C}{\partial t} = \alpha_1 D\,\nabla^2 C + \alpha_2 \frac{D}{RT}\nabla C\nabla v \tag{3}$$

The vacancy concentration around the crack tip is calculated by using FEM according to Eq.(3). The changes of vacancy concentration ahead of the crack tip for GTAW joint model during creep calculated by using $\alpha_2/\alpha_1=300$, $\Delta V=2.0e^{-6}(m^3/mol)$ and $D=1.5\times10^{-9}$, $1.5\times10^{-10}(m^2/s)$ are shown in Figure 17. The vacancy concentration increases to higher level in the center of specimen where multi-axiality is high than that in the specimen surface, when $1.5\times10^{-9}(m^2/s)$ is used as diffusion coefficient. This result is consistent with the experimental one that creep void is often observed in the center of specimen thickness.
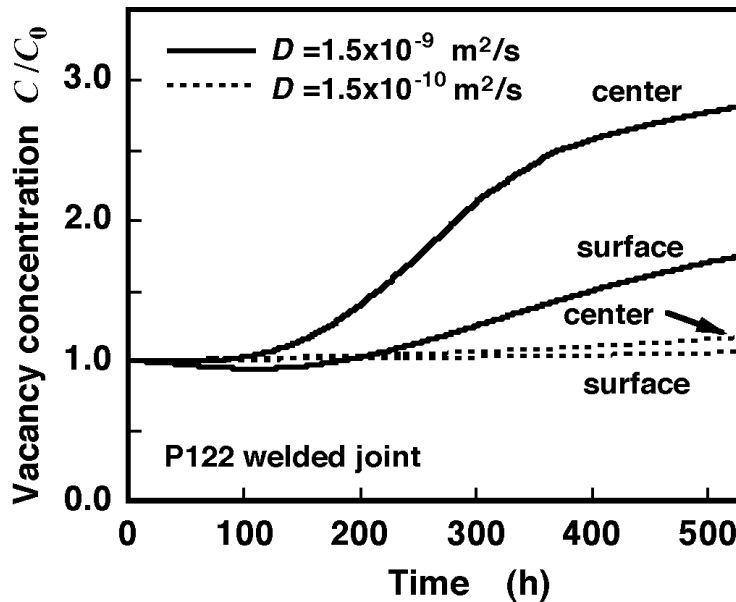

Figure 17   Changes of vacancy concentration ahead of the crack tip for welded joint during creep.

In order to reflect the vacancy calculation to crack growth analysis, here we assume the following computational procedure. When the vacancy concentration reaches to the critical

value, which means the void initiation, the stiffness matrix [K] around the crack tip is decreased as the vacancy concentration increased. We are attempting to simulate creep crack growth by combining the critical strain criteria and vacancy diffusion criteria. Figure 18 shows an example calculated by assuming that the critical vacancy concentration C/C_0 is 1.5. We can obtain the qualitative result that crack initiation time and growth rate is accelerated by taking the void formation ahead of the crack tip into account. The calculating procedure concerning void formation and parameters including critical values for simulation should be further investigated.
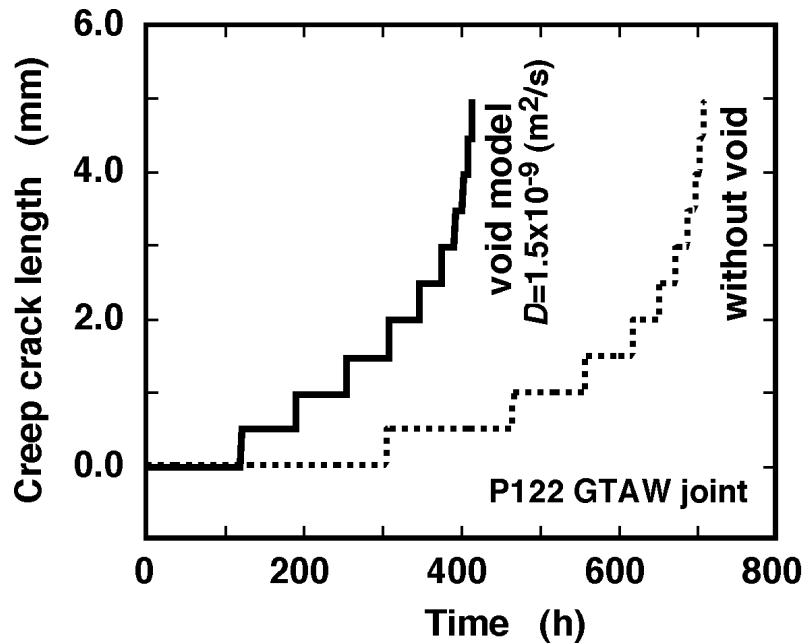
Figure 18   Example of creep crack growth simulation taking the diffusive growth of void into account.

4   SUMMARY

(1) The creep rupture time of simulated HAZ specimens has its minimum after A_{C3} heating which produces fine-grained martensitic microstructure with high density of dislocations. The creep rupture time of the fine-grained HAZ is about one-fifth of the base metal. In the fine-grained A_{C3} simulated HAZ specimens, the coarsening of $M_{23}C_6$ and the inhomogeneous recovery of excess dislocations are significant during creep. The onset of acceleration creep takes place at shorter times in the A_{C3} simulated HAZ specimens than in the A_{C1} simulated HAZ specimens and the base metal. This results in higher minimum creep rate and hence shorter tome to rupture time in the A_{C3} simulated HAZ specimens than in the A_{C1} simulated HAZ specimens and the base metal.
(2) The creep rupture strength of the welded joint is almost the same as that of the base metal at high stress and short time conditions but it decreases rapidly and then it becomes almost the same as that of the A_{C3} simulated HAZ specimen at low stress and long time conditions. The welded joints are fractured in the fine-grained HAZ at low stresses, indicating Type IV fracture. The recovery of high density of dislocations and the sparse distribution of large

$M_{23}C_6$ carbides in the fine-grained HAZ promote the inhomogeneous formation of coarse subgrains during creep. The inhomogeneous recovery of microstructure results in the concentration of creep deformation in the fine-grained zone and hence accelerates eventual creep fracture.

(3) Reducing the width of HAZ by EB welding is effective for the improvement of creep rupture strength of welded joints, although the brittle Type IV cracks appear even in the EBW joints at low stresses.

(4) In both the EBW and GTAW joint specimens, the creep damages initiate near the specimen surface at about half time of life with the crack growing towards the center of specimen thickness. FEM code, which simulates type IV crack growth, has been developed based on the experimental results. The vacancy diffusion under multi-axial stress condition in HAZ of welded joints is calculated. The effect of creep ductility and void formation ahead of the crack tip on creep crack growth rate can be simulated.

REFERENCES

1. F. Abe, H. Okada, S. Wanikawa, M. Tabuchi, T. Itagaki, K. Kimura, K. Yamaguchi and M. Igarashi : *Proc. 7th Liege Conf. on Materials for Advanced Power Engineering*, Liege (2002) 1397-1406.
2. E. Letofsky and H. Cerjak : *Modeling of Microstructural Evolution in Creep Resistant Materials*, The University Press, Cambridge, (1999) 91.
3. Y. Hasegawa, M. Ohgami, Y. Okamoto: *Proc. Advanced Heat Resisting Steels for Power Generation,* San Sebastian, Spain, (1998) 581.
4. K. Ogawa, A. Iseda, Y. Sawaragi, S. Matsumoto and F. Masuyama : *Sumitomo Metals*, **47** (1995) 39.
5. M. Tabuchi, T. Watanabe, K. Kubo, M. Matsui, J. Kinugawa and F. Abe : *J. Soc. Mater. Sci. Japan*, **50** (2001) 116-121. (in Japanese)
6. M. Tabuchi, T. Watanabe, K. Kubo, M. Matsui, J. Kinugawa and F. Abe : *Int. J. of Pressure Vessels and Piping*, **78** (2001) 779-784.
7. M. Matsui, M. Tabuchi, T. Watanabe, K. Kubo, J. Kinugawa and F. Abe : *ISIJ International*, **41** (2001) S126-S130.
8. M. Tabuchi, K. Kubo, T. Watanabe, H. Hongo, M. Matsui and F. Abe : *Proc. 3rd International HIDA and Integrity Conference*, Lisbon, Portugal (2002) 365-374.
9. R. W. Evans and B. Wilshire : *Creep of Metals and Alloys*, The Institute of Metals, London, (1985) pp. 69-113.
10. K. R. Williams and B. Wilshire : *Mater. Sci. Eng.*, **28** (1977) 289-296.
11. M. Matsui, M. Tabuchi, T. Watanabe, K. Kubo and F. Abe : *Proc. 7th Liege Conf. on Materials for Advanced Power Engineering*, Liege (2002) 1691-1700.
12. T. Ogata and M. Yaguchi ; *J. Soc. Mater. Sci. Japan*, **47** (1998) 253.
13. H. Riedel : *Fracture at High Temperatures*, Springer-Verlag, Berlin (1987) 272.
14. K. Yagi, M. Tabuchi and K. Kubo : *Eng. Fract. Mech.*, **57** (1997) 463.
15. K. M. Nikbin, D. J. Smith and G. A. Webster : *Trans. ASME J. Eng. Mater. Tech.*, **108** (1986) 189.
16. T. R. Hsu and Z. H. Zhai : *Eng. Fract. Mech.*, **20** (1984) 521.
17. H.P. Leeuwen : *Eng. Fract. Mech.*, 6 (1974) 141.
18. A. T. Yokobori, Jr., T. Nemoto, K. Sato and T. Yamada : *Japan Soc. Mech. Eng.*, **59** (1993) 104.